

Rotational Temperature Modeling of the Swan $\Delta\nu = 0$ Band Sequence in Comet 122P/de Vico

Tyler Nelson,^{*,†} Anita L. Cochran,^{*,†,¶} and Colin Western[‡]

[†]*University of Texas At Austin*

[‡]*University of Bristol*

[¶]*McDonald Observatory*

E-mail: tyler.neslon@utexas.edu; anita@astro.as.utexas.edu

Abstract

We modeled observations of the C_2 $d^3\Pi_g - a^3\Pi_u$ (Swan) $\Delta\nu = 0$ sequence observed in spectra of comet 122P/de Vico obtained with the 2.7 m Harlan J. Smith Telescope and Tull Coude spectrograph of McDonald observatory on 10/03/1995 and 10/04/1995. The data used spanned 4986-5169 Å at $R = \lambda/\Delta\lambda = 60,000$. We used the PGOPHER molecular spectra model to generate and fit synthetic spectra with the $d^3\Pi_g$ having one and two rotational temperatures. We found the excited state had a two component rotational temperature, similar to that found for comet Halley. The modeled spectrum was sufficiently high quality that local perturbations were important to include. The large perturbation, $b^3\Sigma_g^-(\nu = 10)$, was added to our fits and some new estimates on its molecular constants were found.

Introduction

Comets and asteroids represent the leftovers from the epoch of planet formation within the solar system. Comets differ from the rocky asteroids by the presence of ices, which are a direct indication that they formed in a region beyond Jupiter. Since comets spend most of their orbit in cold regions and have insufficient mass to differentiate or undergo structure-altering

processes, they contain the least altered material from the primordial solar system. Thus, studies of comets offer constraints on conditions in the early solar nebula.

Comets are mixtures of ices and dust, with the mass being split approximately equally between those two substances. The cometary ice is about 80% H_2O , the remainder having contributions from other ices such as CO , CO_2 , CH_4 , NH_3 , etc. As the comet approaches the Sun, the ices are sublimated and flow out from the nucleus carrying dust along with it. The dust quickly disentrains from the gas, flowing outwards more slowly than the gas. The gas travels outwards from the nucleus at a velocity that is dependent on heliocentric distance, being approximately 0.85 km sec^{-1} at 1 AU. Beyond a short distance from the nucleus (500 – 1000 km depending on how active the comet is) the density of the gas is too low for collisions. Thus, the spectra of comets are marked by resonance fluorescence of the molecules excited by sunlight.

We observe only fragment species in the optical region of the spectrum. One of the most prominent set of molecular emissions observed are the $d^3\Pi_g - a^3\Pi_u$ Swan bands of C_2 . The Swan bands are the dominant features in the green, orange and red part of the spectrum. Cometary spectra allow investigation of C_2 with longer path lengths and better vacuum than lab

conditions. Thus, we are using observations of a comet to probe the structure of the C_2 spectrum and to determine the production pathways.

Outside the collisional zone, C_2 can reach high J levels because it has no pure rotational spectrum and only $\Delta J \pm 1$, are allowed for electronic transitions (see Ref. 1). The rotational temperature characterizes the distribution of J levels. Lambert et al.² demonstrated that the observed C_2 Swan (0-0) band of comet 1P/Halley had two rotational temperatures, whereas their observations of an acetylene torch spectrum had only one. These two populations in Halley had temperatures, $T_{\text{low}} = 600 - 700\text{K}$ and $T_{\text{high}} \approx 3200\text{K}$. Previous rotational temperature calculations in comets for C_2 by Lambert and Danks³, A’Hearn⁴, and Danylewych et al.⁵ only were modeled with a single temperature which was similar to the high temperature component of Halley.

In this paper, we present evidence for two rotational temperatures in comet 122P/de Vico using modern spectroscopy modeling software and specifying the $d^3\Pi_g$ population function. This approach has several advantages, including simplicity, uniform treatment of uncontaminated blended lines, and the ability to treat perturbations. We also give estimates on some molecular constants for $b^3\Sigma_g^-(\nu = 10)$, which perturbs the $d^3\Pi_g$ ($\nu = 0$) state for $N = 47$.

Observations

We observed comet 122P/de Vico using the 2.7m Harlan J. Smith Telescope of The University of Texas at Austin’s McDonald Observatory. We used the high-spectral resolution Tull 2Dcoude spectrograph.⁶ The spectra have a resolving power, $R = \lambda/\Delta\lambda = 60,000$ using a slit that was 1.2 arcsec wide and 8.2 arcsec long. Table 1 is a log of the observations.

The comet was relatively bright, resulting in high signal/noise (S/N). In addition, this comet has an extremely high gas-to-dust ratio, resulting in very little continuum from solar photons reflected off the dust. With so little dust, we neglected any solar spectrum removal since it plays such a small part in these observations.

The spectral dispersion of the observations was computed using separate spectra of a ThAr lamp and had an rms error of the wavelength of $\sim 24\text{m}\text{\AA}$. The spectra were Doppler shifted to the laboratory rest frame using the geocentric radial velocity of the comet.

The $\Delta\nu = 0$ band sequence of C_2 is spread over many echelle orders and each order has slightly different sensitivity. We combined the orders together by correcting for the sensitivity variations using a separate solar spectrum obtained with the same instrument. This let us model the $\Delta\nu = 0$ sequence from the (0-0) bandhead at 5165\AA to the (1-0) bandhead at 4737\AA with few strong contaminants. We chose to exclude the $4737\text{-}4783\text{\AA}$ section in the following analysis because it added only a few lines while adding many more noisy data points, thereby degrading the quality of the fit from imperfect noise removal.

Methods

We modeled the de Vico data using the PGO-PHER⁷ molecular modeling code. PGOPHER is a code to model rotational, vibrational and electronic spectra of molecules. It can be used to fit a spectrum of line wavelengths and intensities or, as we used it, to input molecular constants to simulate a molecular spectrum. With its high degree of precision and customization, PGOPHER was well suited for our analysis. Serendipitously, the $\Delta\nu = 0$ band sequence up to (4-4) was already included in a sample constants file making it easy to start our analysis. Brooke et al.⁸ modeled up to (9-9), so we added in their constants to those that came with PGOPHER and have included vibrational levels (0-0) through (9-9) in our models.

Unlike in a laboratory, where a single type of molecule is being studied, the comet spectrum consists of many different molecular emissions (see 9). Thus, the spectral region of the Swan bands can contain contaminants from other species, such as NH_2 . In order that the contaminating lines not influence the quality of the fit, strong contaminating lines were masked out. Many features that were likely perturbed were

also masked out. We further excluded wavelengths less than 4986.2 Å because of persistent offsets between the peaks of the model and data of 0.05 to 0.1 Å. This left 4107 data points covering the wavelength region 4986-5169 Å to model.

Lambert et al.² concluded that the Swan band population of comet Halley represented two different rotational temperatures. It is not clear how universal is the need in cometary spectra for populations at two temperatures. So we tested this by modeling our de Vico spectrum both with a single temperature and with two temperatures. The single temperature version used the built-in simulation temperature. The two-temperature distribution, f , had the form

$$f(a, T_1, T_2) = e^{(-E/(k_B T_1))} + a e^{(-E/(k_B T_2))} \quad (1)$$

where a is the ratio of the contribution of each population, and T_1, T_2 are the two temperatures. In addition, a data scaling factor, a_{spec} , was used for both fits since our data are not flux calibrated. a_{spec} does not change the profile of the modeled spectrum. For both of the rotational temperature distributions, we also included models with and without a vibrational temperature (T_{vib}).

The intensity error is dominated by Poisson noise from the CCD, which is proportional to $\sqrt{\text{Counts}}$ measured, so we use this as a first order weighting scheme. To include these weights in our fit, we made minor modifications to PGOPHER that have been incorporated into the current development version. By including weights, the influence of noise and weak features is reduced.

We also made a preliminary model for the N = 47 perturbation of $d^3\Pi_g(\nu = 0)$ by $b^3\Sigma_g^-(\nu = 10)$. While this perturbation has been suspected since 1963,¹⁰ we could not find the molecular constants required to model it. If unaccounted for, perturbations were a large source of error in our residuals. We used constants from Chen et al.¹¹ as a starting point for $b^3\Sigma_g^-(\nu = 10)$ and adjusted constants until the model achieved a reasonable match with our observations and the identifications given

in Tanabashi et al.¹²

Results and Discussion

The best fit values with 1σ uncertainties and reduced chi-square (χ_r^2) for the one- and two-temperature populations are given in Tables 2 and 3 respectively. The instrumental broadening dominates the line width with a Gaussian FWHM = 0.102 Å. We convolved the models with this broadening to match the data. A model including all relevant perturbations is not available, so a minimum model involving just the states necessary was developed starting with the available constants^{11,12} and adjusting as required. The constants used for the perturbing state are given in Table 4. Visual comparisons of the one- and two-temperature models with the observations in a few important sections are given in Figures 1 and 2. The correlation matrix for the two-temperature fit is given in Table 5. We also used a Markov chain Monte Carlo (MCMC) model¹³ to examine the posterior distributions of the fitted parameters. The a_{spec} parameter was found to be almost identical across all the fits, with a value of 5.26 adopted throughout. The posterior probability distributions for the two-temperature fit are given in Figure 3. The effect of the perturbation is illustrated in Figure 4. While the χ_r^2 values are large for all of the populations used, there is an obvious preference for the two-temperature population. It is also clear that the contribution from the vibrational temperature cannot be excluded, as it improves models with both one and two rotational temperatures. Comparing the residual panels of Figures 1 and 2, it is apparent that the two-temperature model reproduces the (0-0) bandhead better than the single temperature. The one- and two-temperature models were similar for the (1-1) and (2-2) bandheads. We did not see bandheads for (3-3) or higher $\Delta\nu = 0$ transitions. This is not surprising since the (2-2) bandhead is almost washed out by the (1-1) transition, and the (3-3) strength is less than half that of the (2-2).

We investigated the possibility of a three-rotational-temperature population. The fit

with three temperatures was worse than that with two temperatures and actually converged toward the two-temperature solution by driving the coefficient of the third component to zero.

The high value for χ_r^2 that we derive probably comes from either errors in the reduction of the de Vico data or unaccounted physics in the model that we have employed. However, inspection of the figures shows that the fits are quite good in general. Since de Vico has high S/N and low dust, the most likely source of error in the data reduction is order de-tilting. The tilting is most pronounced toward the blue end of the spectrum, which is where the Swan band lines are the weakest and have the least bearing on the quality of the fit. Therefore, we conclude that which physical processes are included/excluded drive our “poor” fit. Small differences in wavelength, usually less than 0.05 Å, between the peaks in the model and data were also seen. All models gave similar residuals around these mismatches so we conclude the temperatures are largely insensitive to this effect. The offsets could result from the peaks falling between two pixels on the CCD.

Inclusion of the $d^3\Pi_g$ $N = 47$ perturbation reduced the χ_r^2 by more than 16% in both models. This seems to be the strongest perturbation but is unlikely to be the only one. For example, the P branch of (1-1) $N = 62$ seems offset, as shown in the right panel of Figure 5. Lambert et al.² saw intensity distributions of some P and R features that did not match the acetylene flame. If this mismatch is a consequence of the different environmental conditions then some deviation would be built in unless the different environments were dealt with explicitly. We removed blends with known contaminants to the best of our ability, but these frequently occur near or within C_2 lines, so a compromise must be reached so that not too much C_2 data is removed. These blends, especially for lines that were completely blended with C_2 , will obviously enhance the observed intensity of the data with respect to the predictions. With many unidentified lines in the our bandpass, the possibility of undiscovered lines that are buried in strong C_2 emission could also exist. We also did not include the Swings¹⁴ effect, in which some lines

that coincide with strong absorptions in the solar spectrum are suppressed since the C_2 band is produced via resonance fluorescence.

Our result agrees with previous work.² We also found that the two-temperature populations extend to the (1-1) and (2-2) bandheads. There are two explanations for this bimodal temperature. Jackson et al.¹⁵ found this as an outcome of the photolysis of C_2H , arguing that either the sudden or phase-space models of dissociation can apply. The sudden model is a classical treatment of the break up, where there is a maximum attainable rotational energy which corresponds to max J. In comparison, the phase-space model proceeds more slowly, allowing all J levels to be accessed. The sudden model gives a low J level distribution because the J values are constrained by classical conservation models, whereas the phase-space model allows for the high J level distribution. Which model applies depends on the trajectory of the H atom along the C_2H potential surface during photodissociation. Communication from Jackson to Lambert in 1989 (see 2) also indicated that a similar bimodal population can result from other parents/grandparents. The other explanation outlined by Lambert et al.² is driven by intercombinational cooling from $c^3\Sigma_u^+ - X^1\Sigma_g^+$ and $a^3\Pi_u - X^1\Sigma_g^+$ transitions. Since the triplet-singlet transitions occur more readily than the singlet-triplet ones there is a net loss of energy from the triplet system. Thus a-X and c-X cool the Swan system. Simulation results by Gredel et al.¹⁶ and Krishna Swamy¹⁷ offer support for this.

Quantifying the importance of the formation pathways versus the intercombinational transitions depends on our ability to distinguish or isolate them. A first attempt could be examining the spectrum as a function of cometocentric distance, assuming that the formation influence diminishes far away from the nucleus. This relies on the time for a C_2 molecule to establish fluorescence equilibrium with the Sun, τ_{eq} . Lambert and Danks³ and O’Dell et al.¹⁸ estimated this value as $\tau_{eq} < 500$ seconds. The lifetime against photodissociation of C_2 at de Vico’s heliocentric distance can be computed using the cometary scale lengths of Cochran¹⁹

of 5.7×10^4 km and an outflow velocity of 1 km sec⁻¹. Thus the expected lifetime of C₂ is of order 5.7×10^4 sec. Once appreciable amounts of new C₂ are no longer made, the contribution from formation should be small.

Jackson et al.¹⁵ produced bimodal temperatures for the X¹Σ_g⁺, A¹Π_u, and B¹Σ_g⁺ singlet states in the laboratory. They found each electronic state has significantly different temperatures. Krishna Swamy¹⁷ predicted that the Mulliken and Phillips systems should also have bimodal temperatures. We intend to investigate whether there are two temperatures in the Phillips system for de Vico observations in a later analysis.

Krishna Swamy¹⁷ seemingly reproduced the two-temperature distribution observed in comet Halley by including Phillips, Mulliken, Ballik-Ramsay, Swan, and the a³Π_u – X¹Σ_g⁺ systems. He assumed all molecules start in the $\nu = J = 0$ ground state and modeled them by exposure to a smoothed solar spectrum. He did not discuss why the photolysis of C₂H would produce this population. Applying either of the aforementioned photodissociation mechanisms implies some initial J distribution. What results from populations with other rotational, vibrational, and electronic levels that emulate cometary conditions is unknown. Krishna Swamy recovered a bimodal distribution without including the c-X transition. Gredel et al.¹⁶ found the rotational temperature strongly depends on both a-X and c-X strengths since both move energy into the singlet system. A simulation, testing different source functions, pressures, and initial population distributions would be of great interest to constrain what the bimodal temperature depends on.

Conclusions

In this paper, we have applied new models of the C₂ Swan band in comet 122P/de Vico. These models fit most of the $\Delta\nu = 0$ band well by incorporating a two-temperature source population as well as including some perturbations between states. We showed that this two-temperature model fits the data better than ei-

ther a single rotational temperature or three rotational temperatures. The reason for the two temperature populations is not entirely clear, though we quote several papers with potential models. We plan to add to our understanding of the processes that produce the C₂ spectrum by using additional observations of comets. We will explore how universal is the two-temperature population with heliocentric distance and cometary orbital dynamical type in future work.

Acknowledgement This work was performed under NASA grant NNX17A186G. TN was supported by the Dean’s Excellence Fellowship.

References

- (1) Herzberg, G. *Molecular Spectra and Molecular Structure: Spectra of Diatomic Molecules*; R.E. Krieger Publishing Company, 1989.
- (2) Lambert, D. L.; Sheffer, Y.; Danks, A. C.; Arpigny, C.; Magain, P. High-Resolution Spectroscopy of the C₂ Swan 0-0 Band from Comet P/Halley. *Astrophys. J.* **1990**, *353*, 640–653.
- (3) Lambert, D. L.; Danks, A. C. High-Resolution Spectra of C₂ Swan Bands from Comet West 1976 VI. *Astrophys. J.* **1983**, *268*, 428–446.
- (4) A’Hearn, M. F. Synthetic Spectra of C₂ in Comets. *Astrophys. J.* **1978**, *219*, 768–772.
- (5) Danylewych, L. L.; Nicholls, R. W.; Neff, J. S.; Tatum, J. B. Absolute Spectrophotometry of Comets 1973XII and 1975IX. II - Profiles of the Swan Bands. *Icarus* **1978**, *35*, 112–120.
- (6) Tull, R. G.; MacQueen, P. J.; Sneden, C.; Lambert, D. L. The High-Resolution Cross-dispersed Echelle White-pupil Spectrometer of the McDonald Observatory 2.7-m Telescope. *Pub. Astron. Soc. Pac.* **1995**, *107*, 251–264.

- (7) Western, C. M. PGOPHER: A Program for Simulating Rotational, Vibrational and Electronic Spectra. *J. Quant. Spectrosc. Radiat. Transfer* **2017**, *186*, 221 – 242, Satellite Remote Sensing and Spectroscopy: Joint ACE-Odin Meeting, October 2015.
- (8) Brooke, J. S.; Bernath, P. F.; Schmidt, T. W.; Bacskay, G. B. Line Strengths and Updated Molecular Constants for the C₂ Swan System. *J. Quant. Spectrosc. Radiat. Transfer* **2013**, *124*, 11 – 20.
- (9) Cochran, A. L.; Cochran, W. D. A High Spectral Resolution Atlas of Comet 122P/de Vico. *Icarus* **2002**, *157*, 297–308.
- (10) Callomon, J. H.; Gilby, A. C. New Observations on the Swan Bands of C₂. *Can. J. Phys.* **1963**, *41*, 995–1004.
- (11) Chen, W.; Kawaguchi, K.; Bernath, P. F.; Tang, J. Simultaneous Analysis of the Ballik-Ramsay and Phillips Systems of C₂ and Observation of Forbidden Transitions between Singlet and Triplet States. *J. Chem. Phys.* **2015**, *142*, 064317.
- (12) Tanabashi, A.; Hirao, T.; Amano, T.; Bernath, P. F. The Swan System of C₂: A Global Analysis of Fourier Transform Emission Spectra. *Astrophys. J., Suppl. Ser.* **2007**, *169*, 472–484.
- (13) Foreman-Mackey, D.; Hogg, D. W.; Lang, D.; Goodman, J. emcee: The MCMC Hammer. *Pub. Astron. Soc. Pac.* **2013**, *125*, 306.
- (14) Swings, P.; Elvey, C. T.; Babcock, H. W. The Spectrum of Comet Cunningham, 1940C. *Astrophys. J.* **1941**, *94*, 320.
- (15) Jackson, W. M.; Blunt, V.; Lin, H.; Green, M.; Olivera, G.; Fink, W. H.; Bao, Y.; Urdahl, R. S.; Mohammad, F.; Zahedi, M. Non-Adiabatic Interactions in Excited C₂H Molecules and their Relationship to C₂ Formation in Comets. *Astrophys. Space Sci.* **1996**, *236*, 29–47.
- (16) Gredel, R.; van Dishoeck, E. F.; Black, J. H. Fluorescent Vibration-Rotation Excitation of Cometary C₂. *Astrophys. J.* **1989**, *338*, 1047–1070.
- (17) Krishna Swamy, K. S. On the Rotational Population Distribution of C₂ in Comets. *Astrophys. J.* **1997**, *481*, 1004–1006.
- (18) O’Dell, C. R.; Robinson, R. R.; Krishna Swamy, K. S.; McCarthy, P. J.; Spinrad, H. C₂ in Comet Halley - Evidence for its being Third Generation and Resolution of the Vibrational Population Discrepancy. *Astrophys. J.* **1988**, *334*, 476–488.
- (19) Cochran, A. L. A Re-evaluation of the Haser Model Scale Lengths for Comets. *Astron. J.* **1985**, *90*, 2609–2614.

Table 1: Log of Observations

Date (UT)	Heliocentric	Geocentric
	Distance (AU)	Distance (AU)
03 Oct 1995	0.66	1.00
04 Oct 1995	0.66	0.99

Perihelion was 06 Oct 1995.

Table 2: Single Temperature Fit Summary

	With Perturbation		Without Perturbation
	Without T_{vib}	With T_{vib}	With T_{vib}
T_{rot} (K)	5075 ± 17	4031 ± 25	3880 ± 30
T_{vib} (K)	-	5860 ± 29	6100 ± 34
χ_r^2	560	406	492

Table 3: Two Temperature Fit Summary

	With Perturbation		Without Perturbation
	Without T_{vib}	With T_{vib}	With T_{vib}
a	1.249 ± 0.034	1.112 ± 0.037	1.313 ± 0.054
T_1 (K)	6130 ± 45	5432 ± 76	5663 ± 103
T_2 (K)	1179 ± 43	931 ± 43	1095 ± 50
T_{vib} (K)	-	5519 ± 25	5674 ± 30
χ_r^2	313	280	360

Table 4: Molecular Constants for $b^3\Sigma_g^-(\nu = 10)$

Origin	19836.25468
B	1.5418643
λ	0.3593
o	-1.498^a
$\gamma \times 10^4$	3.929
$p \times 10^5$	2.1^a
$D \times 10^6$	6.417
$H \times 10^{12}$	4.88^a
Strength	0.03392826

a : Values from Chen et al.

Table 5: Two Temperature Fit Correlation Matrix.

	a	T_1	T_2	T_{vib}
a	1.0	0.779	0.552	-0.290
T_1	0.779	1.0	0.724	-0.478
T_2	0.552	0.724	1.0	-0.224
T_{vib}	-0.290	-0.478	-0.224	1.0

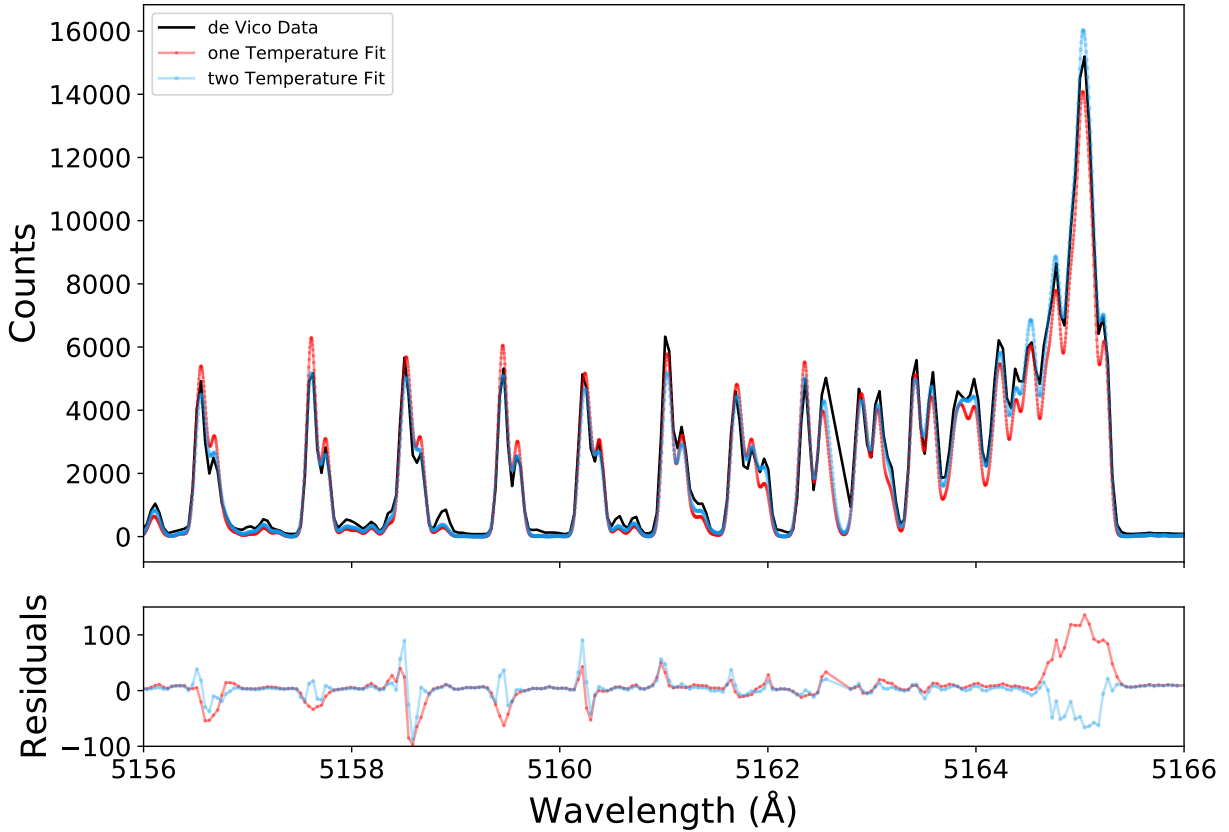


Figure 1: The de Vico data near the (0-0) bandhead is shown along with the one- and two-temperature fits superimposed. While both models fit some parts of this spectral region well, the bandhead is fit better with the two-temperature model.

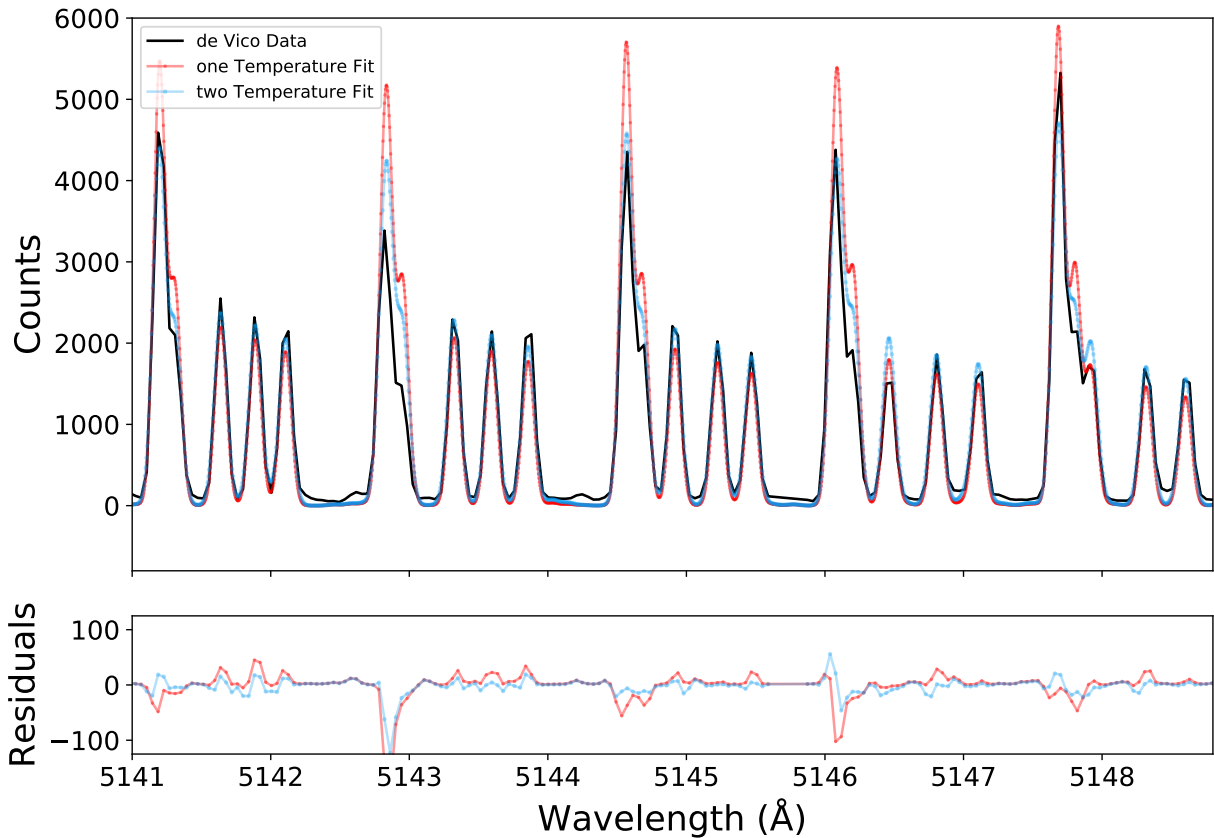


Figure 2: Comparison of the one- and two-temperature fits for some (0-0) P and R branch lines. The strongest lines are from the P branch, while the weaker lines are the R branch. Overall, the two-temperature model fits the data better than the one-temperature model. The P branch line at around 5143 Å is weaker than either model predicts. This might be the result of the Swings effect.

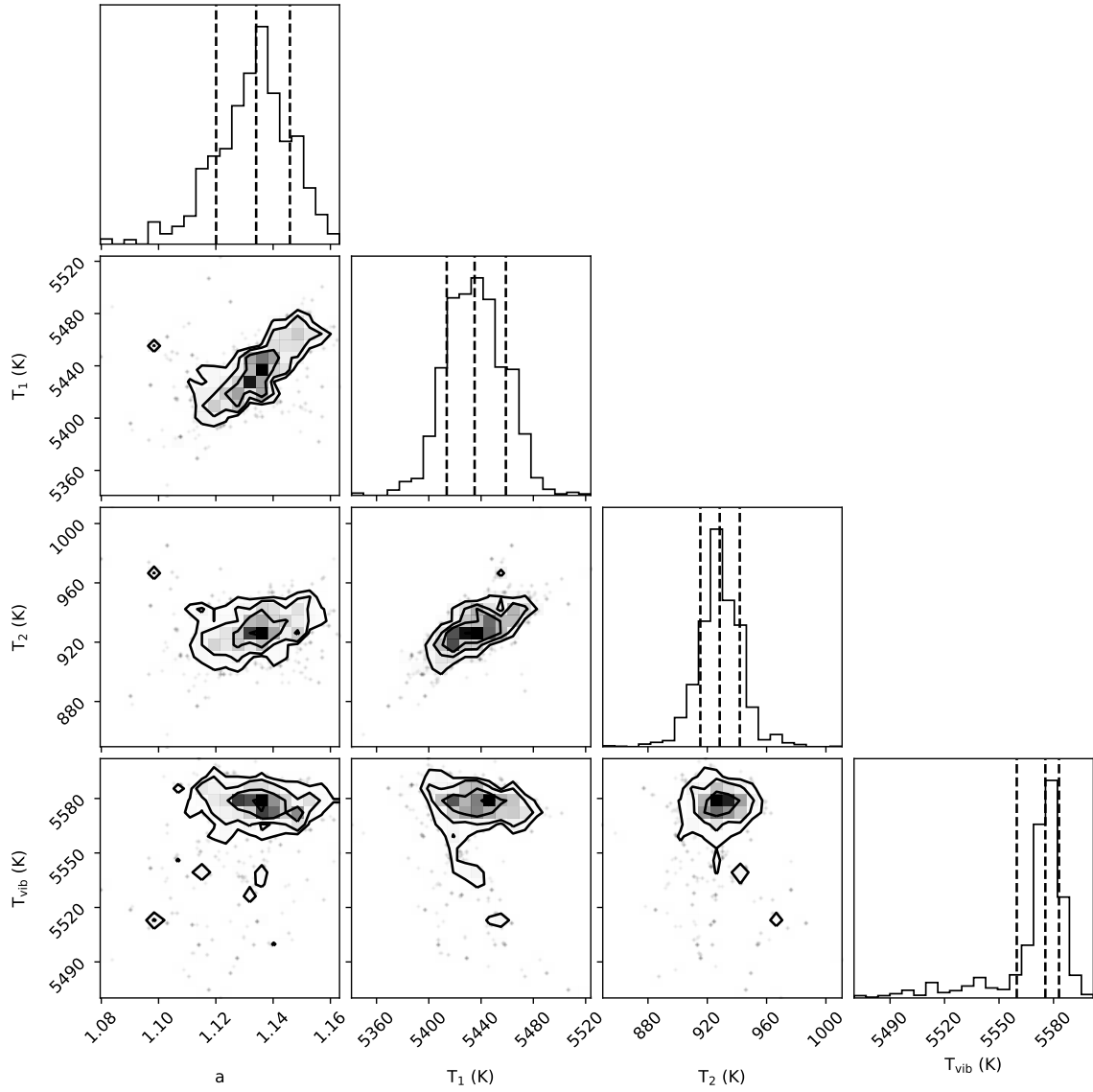


Figure 3: Posterior Probability distributions for two-temperature population. Contours are 1, 2, and 3σ , center dotted line on the histogram is the mean with the other dotted lines indicating the 1σ confidence interval.

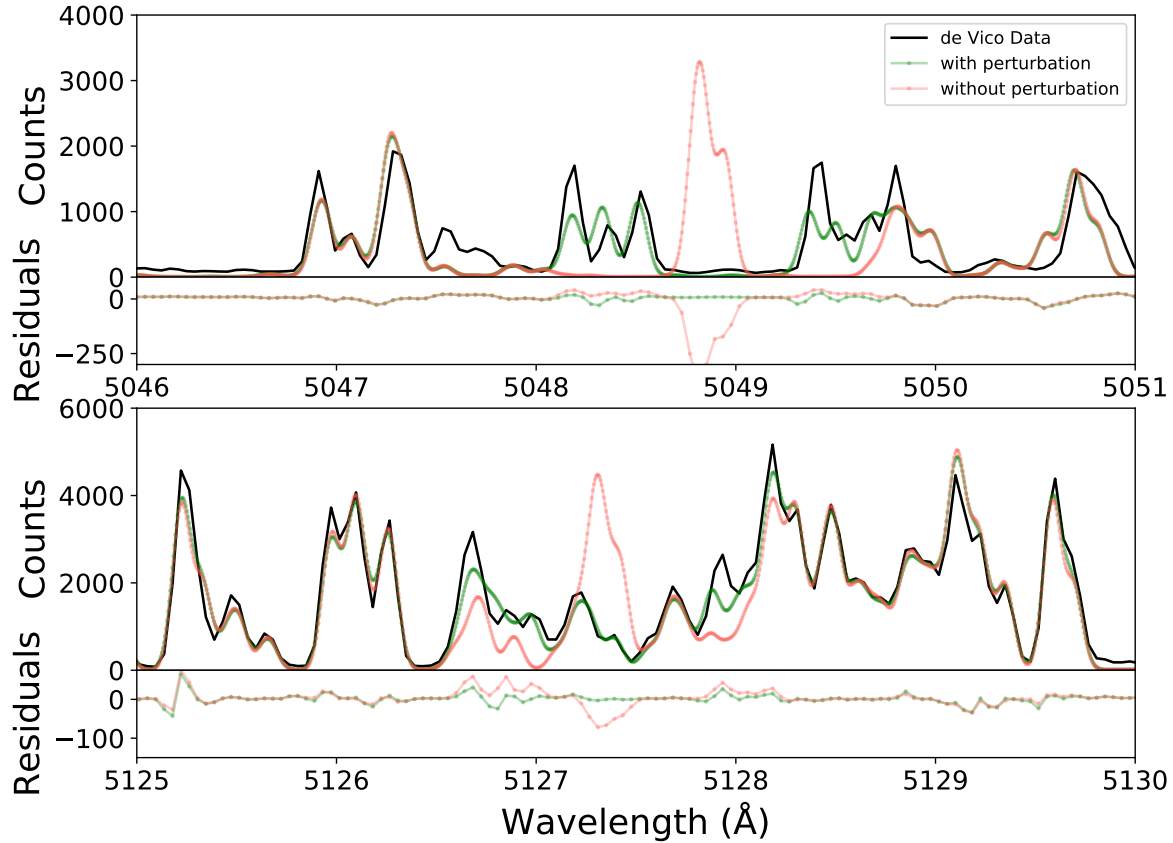


Figure 4: The two-temperature model is shown with and without the $b^3\Sigma_g^-(\nu = 10)$ perturbation included for the R branch (above) and P branch (below). The perturbed model removes the abnormally strong residuals at $N = 47$ seen in the unperturbed system while leaving the rest of the band undisturbed.

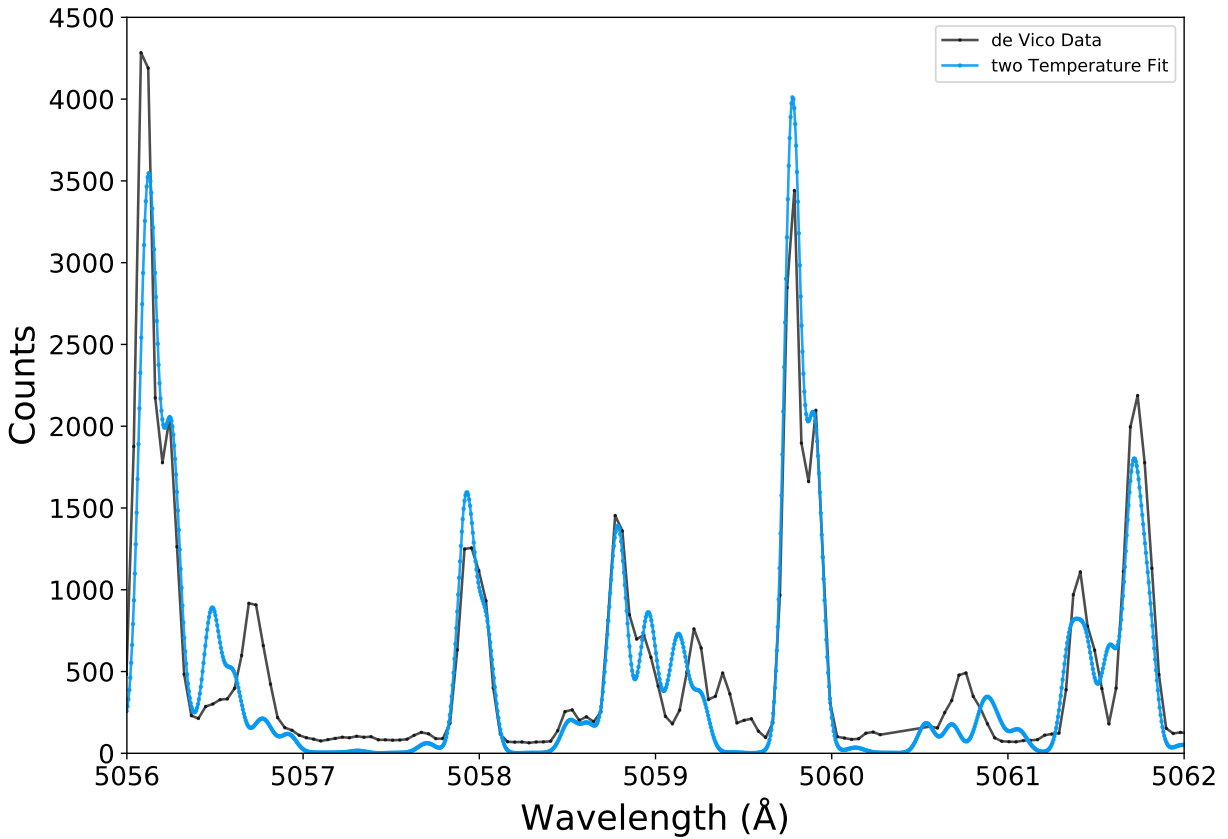


Figure 5: Examples of discrepancies between a two-temperature model and the observed spectrum are shown. Note the apparent shift of the (1-1) emission near 5056.5 Å. It is likely that this shift is the result of perturbations that have not been included in the model.